The Ketogenic Diet Metabolite β-Hydroxybutyrate Promotes Mitochondrial Elongation via Deacetylation and Improves Autism-like Behavior in Zebrafish

Golam M. Uddin[1, 3, 5], Rachel Lacroix[1,3,4,5], Mashiat Zaman[1, 2, 3, 4], Iman Al Khatib[1, 3, 5], Jong M. Rho[6], Deborah M. Kurrasch[1,3,4,5], Timothy E. Shutt [1,2,3,4,5 *]

[1] Cumming School of Medicine, University of Calgary, Calgary, AB, Canada

[2] Department of Biochemistry and Molecular Biology, University of Calgary, Calgary, AB, Canada

[3] Alberta Children's Hospital Research Institute (ACHRI), Calgary, AB, Canada

[4] Hotchkiss Brain Institute, University of Calgary, Calgary, AB, Canada

[5] Department of Medical Genetics, University of Calgary, Calgary, AB, Canada

[6]Departments of Neurosciences, Pediatrics and Pharmacology, University of California San Diego, Rady Children's Hospital, San Diego, CA, USA

Address for Correspondence:

Corresponding Author

Dr. Timothy Shutt

Associate Professor

Email: timothy.shutt@ucalgary.ca

Phone: +1 (403)-220-6114

Abstract

The ketogenic diet (KD) is clinically beneficial and has therapeutic potential access a growing list of neurological disorders, including autism spectrum disorder (ASD). However, the underlying mechanisms mediating the benefits of the KD, which can also have undesirable side effects, remain undefined. To this end, improvements in mitochondrial morphology and function correlate with improved ASD behaviours in response to the KD, though how the KD influences mitochondrial morphology, and whether this is sufficient to improve behaviour remains unknown. Here, we investigate how beta-hydroxybutyrate (βHB), a key metabolite produced by the KD regulates mitochondrial morphology, and whether this pathway could be exploited to improve ASD behaviours. We found that β-oxidation of BHB promotes mitochondrial elongation by increasing NAD^+ levels, which in turn activates SIRT deacetylases that act on key regulators of both mitochondrial fusion and fission. Our data suggest that increasing NAD^+ levels with its precursor, nicotinamide nucleotide (NMN), is sufficient to promote mitochondrial hyperfusion. Finally, both BHB and NMN improve locomotor behaviour in the *shank3*$^{+/-}$ zebrafish model of ASD. Together, our findings elucidate a mechanism by which the ketogenic diet promotes mitochondrial elongation. Moreover, manipulation of this pathway may provide a novel avenue for the treatment of neurological disorders such as ASD, one which may obviate potential complications of the KD in clinical practice.

Introduction:

The high-fat low-carbohydrate ketogenic diet (KD), long appreciated for its clinical efficacy for epilepsy (Neal et al., 2008), is also recognized to have potential beneficial effects in a growing list of diseases. The KD appears beneficial in neurodevelopmental disorders such as autism spectrum disorder (ASD) (Gogou & Kolios, 2018; Napoli, Duenas, & Giulivi, 2014), as well as in neurodegenerative diseases such as amyotrophic lateral sclerosis (Zhao et al., 2006), Parkinson disease and Alzheimer disease (Kashiwaya et al., 2000). Due to its ability to manipulate mitochondrial energy metabolism, the KD may also be effective against cardiovascular diseases (Lopaschuk, Karwi, Ho, Pherwani, & Ketema, 2020), and as a cancer treatment (Weber et al., 2020). Despite the well-documented benefits of the KD, concerns about limitations and complications of the diet are worth noting. For example, compliance with the KD can be challenging, especially in children and adolescents (Lin, Turner, Doerrer, Stanfield, & Kossoff, 2017), with side effects such as gastrointestinal disturbances, nausea/vomiting, diarrhea, constipation, and hypertriglyceridemia being reported (Kang, Chung, Kim, & Kim, 2004). Understanding how the KD works will facilitate the development of alternative approaches that could avoid these complications.

Mitochondria are thought to be a central target mediating the effects of the KD. A key aspect regulating mitochondrial function is their dynamic structure, as they capable of fusing, dividing, and moving about the cell (Shutt & McBride, 2013; Wai & Langer, 2016). These processes influence mitochondrial function, with fragmentation of the mitochondrial network often associated with dysfunction (Baker, Patel, & Khacho, 2019; Glancy, Kim, Katti, & Willingham, 2020). Notably, recent work has shown that the KD can

improve mitochondrial structure and function in the BTBR mouse model of ASD(Ahn et al., 2020), which is consistent with behavioral benefits in mouse models of ASD (Ahn, Narous, Tobias, Rho, & Mychasiuk, 2014; Ruskin, Murphy, Slade, & Masino, 2017; Ruskin et al., 2013), and clinical trials in children (El-Rashidy et al., 2017; Evangeliou et al., 2003; R. W. Y. Lee et al., 2018). However, the underlying mechanism(s) by which KD regulates mitochondrial structure remain unclear.

The ketone body β-hydroxybutyrate (BHB) is a key metabolic product of the KD that is thought to mediate many of the therapeutic effects of the KD (Newman & Verdin, 2017). There are multiple ways through which BHB is proposed to act, including inhibition of histone deacetylases that can elicit changes in gene expression (Shimazu et al., 2013), acting as a signaling molecule via G-protein-coupled receptors (GPCR) (Miyamoto et al., 2019), and as a metabolite consumed by mitochondria to generate ATP. With respect to this latter mechanism, when mitochondria catabolise BHB via β-oxidation instead of glucose, more NAD^+ is available, with less being converted to NADH (Elamin, Ruskin, Masino, & Sacchetti, 2017; Newman & Verdin, 2017). Given that NAD^+ is a necessary cofactor in several important enzymatic reactions, BHB-mediated changes in NAD^+ can impact many cellular and mitochondrial functions. For example, NAD^+ activates the sirtuin deacetylase enzymes (SIRTs) (Bonkowski & Sinclair, 2016; Covarrubias, Perrone, Grozio, & Verdin, 2021), which is a notable phenomenon, as protein deacetylation can mediate mitochondrial elongation (Uddin, Abbas, & Shutt, 2021).

Zebrafish are a valuable model for studying complex brain disorders such as ASD (Kalueff, Stewart, & Gerlai, 2014). Recently, genetic mutant models of verified autism-risk genes have been created and are shown effectively recapitulate autism-like behaviours

(Durand et al., 2007; Liu et al., 2018). *SHANK3*, encodes a master scaffolding protein that has critical roles in synaptogenesis and synaptic function (Monteiro & Feng, 2017), and is a validated ASD-risk gene in humans (SFARI, 2022; Yi et al. 2016). Moreover, *shank3b*$^{+/-}$ deficient zebrafish display core features of ASD-like behaviour, such as impaired locomotor activity, repetitive behaviours and social defects (S. Lee et al., 2018; Liu et al., 2018). Linking SHANK3 to mitochondria and mitochondrial function, mouse models show that the SHANK3 protein interacts with several mitochondrial proteins (Y. Lee et al., 2017). Meanwhile, mice harboring a *Shank3* mutation associated with ASD had elevated S-nitrosylation of mitochondrial proteins, indicative of mitochondrial dysfunction (Kartawy, Khaliulin, & Amal, 2021).

While BHB treatment leads to mitochondrial elongation in cultured cells (Ahn et al., 2020; Santra, Gilkerson, Davidson, & Schon, 2004), it is neither clear how BHB regulates mitochondrial morphology, nor whether BHB alone is sufficient to recapitulate the beneficial effects of the KD on ASD behaviours. Here, we investigated if and how mitochondrial morphology is impacted by BHB-mediated changes in NAD^+, and whether this pathway could potentially be exploited to improve behaviors in a zebrafish model of ASD.

Results:

BHB mediated increase in NAD^+ is necessary to promote mitochondrial elongation:

A 24hr treatment with 5mM βHB promoted mitochondrial elongation in HeLa cells (Figure 1A), as assessed by both quantitative analysis of mitochondrial branch length (Figure 1B), and qualitative analysis of overall mitochondrial morphology via visual scoring (Figure 1C). As BHB is reported to increase NAD^+ via β-oxidation (Elamin et al., 2017), we measured levels of NAD^+ in BHB-treated cells. As expected, treatment with BHB increased the levels of NAD^+ (Figure 1D, Supplementary figure 1B and 2D) and NAD^++ NADH levels (Supplementary Figure 1C and 2E). Notably, blocking β-oxidation using the CPT1a inhibitor etomoxir (Xu, Taylor, Hurd, & Hatch, 2003) prevented both BHB-mediated increases in NAD^+ (Figure 1D) and mitochondrial elongation (Figure 1A-C, Supplemental Figure 2A-C), suggesting that β-oxidation is required for BHB to increase NAD^+ levels, and that increased NAD^+ is required for βHB-induced mitochondrial elongation.

Increased NAD^+ is sufficient to promote mitochondrial elongation:

To investigate whether increased NAD^+ alone could promote mitochondrial elongation, we treated cells with the NAD^+ precursor molecule nicotinamide mononucleotide (NMN). Similar to the BHB treatment, we found that the NMN is able to increase both NAD^+ levels (Figure 1D) and NAD^++ NADH levels (Supplementary Figure 1C), as well as promote mitochondrial elongation (Figure 1A-C).

BHB and NMN promote mitochondrial elongation by increasing mitochondrial fusion and decreasing mitochondrial fission:

Mitochondrial elongation can be caused by either increased fusion and/or decreased fission (Sabouny & Shutt, 2020). To investigate how BHB and NMN promote mitochondrial elongation, we examined key proteins mediating both mitochondrial fusion and fission (Figure 2A-D, Supplemental Figure 1D-G). We found that expression of the OPA1 fusion protein was increased significantly by treatment with BHB, but not NMN. Meanwhile, both BHB and NMN treatments reduced phosphorylation of DRP1 at position serine-616, which is a well-characterized post-translational modification that promotes mitochondrial fission (Sabouny & Shutt, 2020; Uddin et al., 2021). Notably, we did not see any significant changes due to BHB or NMN treatment in DRP1 phosphorylation at serine-637, which inhibits mitochondrial fission (Sabouny & Shutt, 2020; Uddin et al., 2021), nor in the total expression of other key mitochondrial fusion (MFN1, MFN2) or fission (MFF) proteins (Supplementary Figure 1D-G).

As peroxisomes share the same fission machinery with mitochondria, but do not undergo fusion with one another, we next examined if BHB and NMN also impacted peroxisomal morphology through inhibition of peroxisome fission. Curiously, while BHB supplementation increases peroxisome size, NMN supplementation had no effect, suggesting the any effects of BHB on peroxisome morphology was independent of NAD^+ (Fig 2E-F). Supporting this notion, blocking β-oxidation with etoxomir treatment did not impact BHB-induced enlargement of peroxisomes. We also noted that BHB, but not NMN, induced a marked increase in the number of peroxisomes (Fig 2G), consistent with a role for BHB in promoting peroxisome biogenesis independent of its NAD^+-mediated effects.

Next, we interrogated protein acetylation since increased NAD^+ promotes protein deacetylation, a post-translational modification linked to changes in mitochondrial morphology (Uddin et al., 2021). Notably, deacetylation of mitochondrial fusion proteins MFN1, MFN2, and OPA1 is reported to promote mitochondrial fusion (Biel et al., 2016; Lee et al., 2014; Samant et al., 2014), while deacetylation of DRP1 is linked to decreased fission (Hu et al., 2020). As expected, we found that BHB and NMN both reduce global protein acetylation (Figure 3A and B). More specifically, we observed decreased acetylation of OPA1 and DRP1 (Figure 3A, C and D), but were unable to detect any acetylation of MFN1/ MFN2 proteins.

BHB and NMN control mitochondrial morphology via sirtuin-based deacetylation activity:

To determine if NAD^+-mediated protein deacetylation is important for promoting mitochondrial elongation induced by BHB and NMN, and whether sirtuin deacetylases are involved, we examined the effects of sirtinol, an inhibitor of both Sirt1 and Sirt2 (Mai et al., 2005). Treatment with 50µM sirtinol increased global acetylation (Supplementary Figure 2 G-H) and caused an accumulation of NAD^+ (Supplementary Figure 2I), indicating that the inhibitor was functional. Sirtinol treatment also led to fragmentation of the mitochondrial network (Figure 4A-C), consistent with increased protein acetylation levels correlating to mitochondrial fragmentation. Critically, sirtinol treatment prevented BHB and NMN-induced mitochondrial elongation (Figure 4A-C), implicating a role for Sirt1 and/or Sirt2 in BHB and NMN-induced mitochondrial elongation.

Sirt2 is required for NAD^+ induced mitochondrial elongation via BHB:

To determine if Sirt1, Sirt2, and/or Sirt3 is required for BHB or NMN induced mitochondrial elongation, their expression was knocked-down separately via siRNA (Figure 5, Supplementary Figure 3-5). To control for off-target effects, we used three different siRNA targets for each gene, and confirmed knockdown via western blotting (Figure 5D). Upon examining mitochondrial morphology, we observed a similar trend of mitochondrial fragmentation for 2 of the 3 siRNA targets for Sirt1(siRNA#1&2), Sirt2 (siRNA#2&3) and Sirt3 (siRNA#1&3) (Supplemental Figures 3, 4 and 5), again consistent with the notion that deacetylation promotes mitochondrial elongation. As the results from Sirt1 siRNA#3, Sirt2 siRNA#1 and Sirt3 siRNA#2 were not consistent (possibly due to off-target effects), they were discarded for our interpretation. Overall, we found that BHB-induced mitochondrial elongation was unaffected by Sirt1 and Sirt3 knock-down but was abolished by Sirt2 knock-down. Meanwhile, knock-down of either Sirt1 or Sirt2 prevented an NMN-induced mitochondrial hyperfusion phenotype, while Sirt3 knock-down had no effect. However, it should be noted that Sirt3 knockdown was less efficient, and that there could still be residual protein activity. Together, our findings indicate that Sirt2 is required for both BHB- and NMN-induced mitochondrial elongation via increased NAD^+ levels. Meanwhile, the fact that BHB, but not NMN, can induce mitochondrial elongation in the absence of Sirt1 suggests that BHB can also induce mitochondrial elongation via an NAD^+-independent mechanism, consistent with the fact that BHB, but not NMN, increased OPA1 expression.

Both BHB and NMN restore locomotion in a *shank3b*$^{+/-}$ zebrafish model of ASD:

To examine the efficacy of BHB or NMN *in vivo* to alleviate behaviors associated with ASD, we studied their effects in *shank3b*$^{+/-}$ zebrafish. Wild-type control and s*hank3b*$^{+/-}$ fish were exposed to vehicle, BHB, or NMN over the neurogenic developmental timepoint (10-48 hpf (hour post fertilization); Figure 6A). Behaviours were examined at 5 dpf (day post fertilization) by measuring total movement in light and dark (Figure 6C, D). Specifically, *shank3b*$^{+/-}$ fish showed reduced movement in both dark (Figure 6C) and light (Figure 6D); compared to *shank3b*$^{+/+}$ (wild-type) fish exposed to vehicle, consistent with a behavioral movement deficit. Interestingly, in *shank3b*$^{+/-}$ fish, BHB restored movement in light and dark conditions to the levels of wild-type control fish (Figure 6 C-D). NMN restored movement in both light and dark, with a stronger response observed in the dark (Figure 6C, green bars). This finding suggests that either treatment is effective in restoring activity to or above the baseline of wild-type, vehicle exposed fish. Unexpectedly, we saw that βHB alone had an effect in wild-type fish under light conditions, significantly decreasing locomotion compared to vehicle-exposed controls (Figure 6D). This decrease was not observed in wild-type fish exposed to NMN, suggesting that there are some differences between the mechanism(s) through which BHB and NMN elicit their effects. Combined, these findings indicate that decreased movement in *shank3b*$^{+/-}$ zebrafish is restored upon developmental exposure to either BHB or NMN.

Discussion

Our findings provide novel insights into the mechanism by which the KD promotes mitochondrial elongation and suggest that this pathway might be a promising avenue for improving ASD behaviours. The data herein support a model by which β-oxidation of the KD metabolite BHB increases NAD^+ levels to activate sirtuins, which in turn deacetylate key mitochondrial dynamics proteins to promote mitochondrial hyperfusion.

Pathways that modulate mitochondrial morphology often act reciprocally on both fission and fusion, such that mitochondrial hyperfusion is a result of both decreased fission and increased fusion (Sabouny & Shutt, 2020). This situation is true in response to decreased acetylation (Uddin et al., 2021), and our data show this is mirrored by BHB and NMN treatments. With respect to increased fusion, both BHB and NMN reduced OPA1 acetylation, which promotes mitochondrial fusion (Samant et al., 2014; Sheng & Cristea, 2021). While previous work has shown that deacetylation also activates mitochondrial fusion proteins MFN1 and MFN2 (Lee et al., 2014; Oanh, Park, & Cho, 2017), we were unable detect acetylation of these proteins to see how they behaved. Meanwhile, both BHB and NMN also reduced DRP1 acetylation, which is known to reduce fission (Hu et al., 2020). Though the mechanism by which deacetylation reduces fission is unknown, it is tempting to speculate that the acetylation status of DRP1 influences the pro-fission phosphorylation at serine-616 of DRP1. This notion is supported by reduced levels of $DRP1^{P616}$ with both BHB and NMN treatments in this study, and previous work showing NMN treatment decreased $DRP1^{P616}$ in mice hippocampal tissues (Hu et al., 2020; Klimova, Long, & Kristian, 2019), as well as our previous findings of reduced $DRP1^{P616}$ in mouse brains following 2 weeks on the KD (Ahn et al., 2020).

To further investigate the mechanistic pathway by which NAD^+ mediates deacetylation of proteins mediating mitochondrial dynamics, we interrogated the role of Sirt1 and Sirt2, which both localize to the cytosol where they can act on DRP1, as well as Sirt3, which localizes inside of mitochondria where it can act on OPA1. While Sirt3 knockdown did not affect either BHB or NMN-mediated hyperfusion, it is notable that we did not achieve a high reduction in Sirt3 protein levels, and that residual Sirt3 protein could still be active. Meanwhile, knockdown of both Sirt1 and Sirt2 prevented NMN-induced mitochondrial hyperfusion, while only Sirt2 knockdown inhibited BHB-induced mitochondrial hyperfusion. This discrepancy could be due to the fact that BHB has multiple mechanisms of action beyond the novel pathway we have shown here for protein deacetylation via NAD^+ and sirtuins (Newman & Verdin, 2014).

In this regard, we also observed other notable differences between BHB and NMN treatments. First, while BHB increased OPA1 protein levels, NMN did not. This observation is similar to previous work in mouse hippocampal tissues where NMN elevated NAD^+ levels but did not change OPA1 expression (Klimova et al., 2019). Given that NMN increases NAD^+ levels, but not total OPA1 protein, we suggest that the elevated OPA1 expression from BHB supplementation is independent of NAD^+ changes. Another difference between BHB and NMN was with respect to peroxisome morphology, which was investigated because mitochondria and peroxisomes share the same fission machinery. We propose that the increased peroxisome size and abundance with BHB treatment is likely due to the BHB induction of peroxisome proliferator-activated receptors (PPARs), rather than increased NAD^+. This conclusion is based on the observations that etomoxir did not prevent BHB-induced peroxisome elongation, and that NMN had no

effect on peroxisome size. Moreover, BHB-induced increases in peroxisome abundance would be consistent with the known role of PPARs in promoting peroxisome biogenesis and activating β-oxidation (Dreyer et al., 1993; Hess, Staubli, & Riess, 1965). This alternative pathway likely involves the ability of BHB to inhibit histone deacetylases HDAC1, 3 and 4 (Newman & Verdin, 2014; Shimazu et al., 2013), as HDAC3 inhibition activates PPARγ (Galmozzi et al., 2013).

The finding that changes in global acetylation and decreased levels of DRP1^{P616} do not impact peroxisome fission was somewhat unexpected, given the role of DRP1 in the fission of both these organelles. However, this finding is consistent with recent work showing that loss of CLUH did not affect peroxisomal fission despite reducing mitochondrial recruitment of DRP1 and mitochondrial fission (Yang et al., 2022). These unexpected observations suggest that there are discrepancies in how DRP1 regulation impacts both mitochondrial and peroxisomal fission, with DRP1^{S616} affecting mitochondrial fission, but not peroxisome fission

While inhibiting mitochondrial fission or improving mitochondrial fusion alone can improve mitochondrial function in several preclinical disease models (Whitley, Engelhart, & Hoppins, 2019), it is important to note that we see global decreases in protein deacetylation, not just for mitochondrial fission and fusion proteins. Thus, the benefits of promoting protein deacetylation likely go beyond simply just promoting mitochondrial hyperfusion. Additionally, it should be noted that NAD^+ is a critical cofactor for many additional important enzymes that could also contribute to improving mitochondrial function. Consistent with this notion, NAD^+ supplementation is emerging as a popular

therapeutic strategy in many diseases (Bonkowski & Sinclair, 2016; Gilmour et al., 2020; Uddin et al., 2021).

There is growing evidence that mitochondrial dysfunction, which often correlates with mitochondrial fragmentation, is likely to contribute to ASD (Citrigno et al., 2020; Pecorelli et al., 2020; Rossignol & Frye, 2012; Singh et al., 2020; Thorsen, 2020; Weissman et al., 2008). For example, ASD patient cells (Barone et al., 2021; Frye et al., 2021; Gevezova et al., 2021) and brain organoids (Ilieva et al., 2022) exhibit impaired mitochondrial bioenergetics, while postmortem brains of control and ASD patients have increased expression of mitochondrial fission proteins and decreased expression of mitochondrial fusion proteins (Tang et al., 2013). This correlation is also present in animal models of ASD, as neuronal mitochondria in the BTBR mouse model of ASD have reduced mitochondrial function and are more fragmented (Ahn et al., 2020). However, despite the benefits of the KD for ASD behaviors in human studies (El-Rashidy et al., 2017; Spilioti et al., 2013) and in animal models (Y. Ahn et al., 2020), we do not as yet fully understand how the KD provides these benefits, as it has many potential modes of action.

Our finding that either BHB or NMN improve the locomotion behaviour of *shank3b*$^{+/-}$ fish, begins to provide insight into the behavioural benefits of the KD, and is noteworthy for several reasons. First, the fact that βHB alone is beneficial suggests that administration of the full KD may not be necessary. Second, the fact that NMN alone is beneficial suggests that the ability of BHB to increase NAD^+ is important for its benefits. Third, the fact that there are some differences in the effects of BHB and NMN, both at the cellular level and at the behavioural level, suggests that BHB has additional mechanisms

of action beyond increasing NAD^+ that may also impact behaviour. In this regard, it might be interesting to examine the combined effects of BHB and NMN. Finally, if the benefits of BHB and/or NMN in *shank3b*$^{+/-}$ fish are translatable to humans, then administration of BHB or NMN could be a promising approach that bypasses many of the side effects of the KD. However, while it is tempting to propose BHB or NAD+ boosting treatments for ASD, it should be noted that the locomotion assay alone cannot capture the complex behaviours that define ASD. As such, more *in vivo* work with both BHB and NMN is required to characterize their effects on additional animal behaviours.

The elucidation of a novel pathway to regulate mitochondrial morphology is an important advancement, given the critical importance of these processes in mediating mitochondrial function, and the increasingly recognized role that mitochondrial dysfunction plays in many disease (Chan, 2020; Whitley et al., 2019). Moreover, restoring the balance between fusion and fission, either by inhibiting fission or by promoting fusion, is beneficial in several neurological disease models. However, there are currently no established direct therapeutic approaches that target mitochondrial fission or fusion in humans. Despite the promise of the KD in this regard, its use may remain somewhat limited due to the risk of undesired side effects and complications. Thus, our findings that BHB and NMN treatments can recapitulate some of the beneficial effects of the KD, have promising therapeutic potential.

Limitations of the study

In the current study, we set out to explore the mechanisms underlying KD-mediated mitochondrial hyperfusion and improvement in ASD behaviours. We identified a mechanistic pathway linking BHB, a key metabolite of the KD, to increased NAD^+ levels and mitochondrial hyperfusion, but there are limitations to our study. For example, it is important to note that both BHB and NAD^+ have multiple mechanisms of action that likely impact mitochondrial form and function beyond the pathway that we have eluciated. Meanwhile, as we did not obtain robust knockdown of Sirt3, we cannot make definitive conclusions about its role in mediating fusion in response to increased NAD^+. With respect to ASD-related findings, the *Shank3*$^{+/-}$ fish model is only one ASD model, and it remains unclear whether these finings will extend to other ASD models, let alone to human ASD patients. Furthermore, we have only examined locomotor behaviour, which does not fully recapitulate the full extent of ASD behaviours, and have only examined one timepoint using a single dose for BHB and NMN. In this regard, testing additional dosing regimens and behaviours would be important to examine in future studies.

Methods and Materials

Cell Culture: HeLa cells were grown in DMEM, high-glucose media (Cat#11965092, Gibco, USA) containing l-Glutamine and supplemented with 10% fetal bovine serum (FBS). Cells were seeded at 1 x 10^6 cells in 10cm plates and grown at 37 °C and 5% CO_2 until they were 70-80% confluent (approximately after 48 hrs) before being harvested for analysis or re-seed. At a 50-60% confluency (approximately after 18-24 hrs), cells were treated with β-HB (5mM) (Cat#H6501; Sigma, USA) or NMN (50mM) (provided by Dr. David Sinclair) or etomoxir (20µM) (Cat#509455; Calbiochem, Sigma, USA) or sirtinol (1mM) (Cat#566321; Calbiochem, Sigma, USA) for 24hr. In case of experiments where two drugs treated together, both drugs were supplemented in the media together. 24hr post treatment, cells were harvested by washing with 1x PBS, followed by incubation with 0.25% Trypsin (Corning® Trypsin containing 0.1% EDTA; Fisher Scientific) for 1 min at 37°C and 5% CO_2. Detached cells were collected in fresh media, followed by centrifugation at 5000 RPM for 5 min, and cell pellets were then stored at -20^0C for further experiments. Cells used for immunofluorescence were grown on glass coverslips (no. 1.5 -- 12mm diameter; Electron Microscopy Sciences) that were placed in the same 10cm dishes used for protein analysis.

Immunofluorescence Staining: Cells on coverslips were fixed in 4% paraformaldehyde for 15 min at 37 °C, permeabilized with 0.1% TritonX100, and blocked with 10% FBS in PBS as described previously (Ahn et al., 2020). Mitochondria were labelled with TOMM20 (Cat#186735; Abcam, USA) primary antibodies were used at 1:1000, diluted in 10% FBS in PBS, and cells were incubated overnight at 4 °C. The

appropriate secondary AlexaFluor antibodies were diluted in 10% FBS in PBS at 1:1000, and cells were incubated in the dark at room temperature for 1hr. Stained cells were then washed in 1X PBS and mounted using Dako mounting media (Cat#S3023, Agilent, USA).

For peroxisome staining, the cells fixed on the coverslips were permeabilized with 0.1% NP-40 dissolved in 1X PBS for 15 minutes at room temperature. This was washed off with PBS and subsequently, 10% FBS was used to block for one hour at room temperature. Following blocking, an overnight incubation was performed to label the peroxisomes with anti-PMP70 (Cat#P0497, Sigma-Aldrich; 1:1000 dilution in blocking solution). The slips were washed three times with PBS before the complementary anti-rabbit secondary antibody was added (Cat#A-11034, Life Technologies; 1:1000 dilution in blocking solution) and incubated for one hour at room temperature. A final washing step with 1X PBS followed and the slips were mounted using the aforementioned mounting media.

Microscopy and Image Morphology Analysis: An Olympus spinning disc confocal system (Olympus SD OSR, Olympus Corporation, Tokyo, Japan) (UAPON 100XOTIRF/1.49 oil objective) operated by Metamorph software was used to image fixed cells. Mitochondrial network morphology was assessed in a blinded fashion and assigned to 3 categories of mitochondrial morphology (fragmented, intermediate, and fused). A representative image under each category is shown in Supplementary Figure 1A. At least 80-150 cells were counted per condition, and the analyses were performed on 3 independent replicates and 2 independent technical replicates for knockdown study for

each treatment condition. Mitochondrial branch length was quantified using the Image-J, MiNA (Valente, Maddalena, Robb, Moradi, & Stuart, 2017) plug-in from three independent replicates, using a standard region of interest (ROI) and measured randomly from each image.

For peroxisome analysis of the various treatments, Z-projections were obtained, and images adjusted for threshold, the threshold was set to remove any background signals using Image J. Z projections were generated for average intensity using Image J. The Image J particle analysis tool was used to measure peroxisome size, and counts. For peroxisome size analysis, peroxisomes from 200 cells were analyzed and the sizes binned as follows: elongated (0.2-1) μm^2, intermediate (0.1-0.2) μm^2 or round (0.01-0.1) μm^2. Meanwhile, the mean number of peroxisomes was calculated per cell, Sample size is 88 cells in total- 2 biological replicates so 44 cells from each replicate

Western blots: Frozen cell lysates were homogenized using RIPA Lysis and Extraction Buffer (Cat#89900, Thermo Fisher, USA) and protease inhibitors cocktail (Cat#10190-060, VWR, USA), on ice for 1hr. Protein content was measured using Pierce™ BCA Protein Assay Reagent A (Cat#23228; Thermo Fisher, USA) and Pierce™ BCA Protein Assay Reagent B (Cat#23224; Thermo Fisher, USA). Depending on the target, 30–40-µg total protein was loaded onto SDS-PAGE for western blotting. Polyvinylidene fluoride (PVDF) membranes were blocked with 5% nonfat milk in Tris-buffered saline solution containing 0.1% Tween 20 (TBS-T) for 1 h. After blocking, the blots were incubated with primary antibody overnight at 4°C. After washing with TBS-T, the blots were incubated with the secondary antibody for 1 h at room temperature. After

washing with TBS-T, blots were visualized using an SuperSignal™ West Femto Maximum Sensitivity Substrate (Cat#34095; Fisher Scientific, USA). Bands were detected and quantified using a ChemiDOC MP gel imaging system (Bio-Rad). The following antibodies were used: Actin (Cell Signaling; 1:10,000); DRP1 (BD Biosciences, San Jose, CA, USA; 1:1000); pDRP1^{S616} at (Cell Signaling, Danvers, MA, USA; 1:1000); OPA1 (BD Biosciences; 1:1000); MFN1 (Cat# 3455S, Cell Signaling, USA; 1:1000) ; MFN2 (Cat# M03, Abnova, USA; 1:1000); MFF (Cat#, Cell Signaling, USA; 1:1000); and DRP1 S637 (Cat# 4867SS, Cell Signaling, USA; 1:1000). The expression levels of proteins were normalized to actin for cell lysate, and the ratio of the phosphorylated and total forms was computed using the normalized relative total expression levels. Original blots that were used to crop representative are shown in supplementary figure 6: (A-F)

Immunoprecipitation: Freshly centrifuged cell pallet from the cell lysate collected after the 24hr treatment (as described in cell culture section) from a 10cm dish. 250ul of IP homogenization buffer was used to extract proteins. A custom homogenized buffer was prepared for IP sample homogenization, 150mM NaCL (Cat#BP358212; Fisher Scientific, USA), 50mM Tris-HCL at 7.5pH (Cat#97063-756; VWR, USA), 5mM EDTA at 8pH (Cat#E3889; Sigma Adrich, USA), 0.5% NP-40 (Cat#00000; Company), and 1% TritonX (Cat#X100; Sigma Adrich, USA); with freshly added Trichostatin A 1uM (Cat#A8183; ApexBIO, USA), Nicotinamide 5mM (Cat#N0636; Sigma Adrich, USA), 10mM Sodium Butyrate (Cat#303410; Sigma Adrich, USA) and Protease inhibitor cocktail 1:100 (Cat#M250; Amresco, USA). After 1 hr of incubation, samples were centrifugated at 10000 RPM. Supernatant was diluted accordingly to prepare same amount of protein

(350-400ug) and volume (200ul) followed by protein quantification. Preclearing and washing cell lysate were performed using 20ul A/G PLUS-Agarose beads per 200ul sample (Cat#SC2003; Santa Cruz Biotechnology, USA) for 4 hrs followed by centrifugation at 15,000g for 10 minutes at 4^0c. 20ul of collected supernatant was kept separately to use as input. The leftover supernatant was then incubated with 1.5 µL anti-acetyl-lysine antibody (Cat#9441S; Cell signalling, USA) overnight. 60-70ul (depending on the protein concentration used in the beginning) A/G PLUS-Agarose beads were added to the antibody incubated samples. Followed by a 4hr rotation and incubation at 4°C, samples were centrifuged at 5,000g for 5 minutes. Supernatant was discarded and the beads pallet was then washed 3 times with the IP homogenization or extraction buffer with all the components. Washing was performed at at 5,000g for 5 minutes each time. Pallets were then heated at 95°C for 5 min with Laemmli buffer (Cat#1610747; Biorad, USA) and centrifuged at 15,000g for 10 minutes to collect the supernatant. This supernatant was used to perform immunoblotting. Input was prepared checked in a separate gel but same day and setup. Also, a pooled samples (10ul/sample/group) from all groups ran to show as a positive control, 1 sample input /group was used to run together with IP sample to show the differences. IP sample successfully showed heavy chain and light chain produced due to the A/G bead's reaction. Original blots that were used to crop representative are shown in supplementary figure 6: (A-F)

NAD assay: NAD^+ and NADH were measured as described previously (Zhu & Rand, 2012). Briefly, samples were homogenized in extraction buffer (10 mmol/l Tris/HCl, 0.5% Triton X-100, 10 mmol/l Nicotinamide, pH 7.4) and then centrifuged (12,000 × g for 5 min

at 4◦C), after which an aliquot of supernatant was taken for protein quantification. After subsequent extractions with phenol: chloroform: isoamyl alcohol (25:24:1) and chloroform, the supernatant was separated in two aliquots to measure total NAD or NAD+ using a Bio-Rad Imark microplate reader. Data are presented as pmol of NAD^+ or NADH per mg of protein.

siRNA knockdown: TriFECTa RNAi Kits (Integrated DNA Technology, USA) were obtained for SIRT1 (hs.Ri.SIRT1.13), SIRT2 (hs.Ri.SIRT2.13) and Sirt3 (hs.Ri.SIRT3.13). Both a transfection control (TYE563 DsiRNA) (Cat#51-01-20-19), and a negative control DsiRNA (a nontargeting DsiRNA that has no known targets in human, mouse, or rat) (Cat#51-01-14-03), were provided with the kit. 24hrs after siRNA transfection, vehicle, BHB or NMN treatments were initiated, and carried out an additional 24hr. Lipofectamine™ RNAiMAX (Cat#13778075, Thermo Fisher Scientific, USA) was used as transfection reagent. Cells were platted at $0.5x10^5$ density in a 6 well plate. After 12 hrs of seeding, RNAiMAX (9µl/well) and siRNA (100pmol/well) was diluted in Opti-MEM medium (Cat#31985062, Thermo Fisher Scientific, USA). The mixture of RNAiMAX and siRNA was then added to the well for 24hr. Cells were then collected for western analysis and immunfluorescence to analyse mitochondrial morphology as above.

Zebrafish husbandry, behaviour and genotyping: Zebrafish heterozygous for a shank3b mutation (shank3b$^{+/-}$) were placed in breeding tanks the afternoon prior to day 0 of the experiment. Males and females were separated by a removable insert, which was removed the morning of the next day to allow breeding. Embryos were consequently

collected in petri dishes at a density of ~50 embryos/plate and maintained in E3 medium (60X E3 and methylene blue, diluted in milli Q water) at 28°C. At 10 hours-post fertilization (hpf), zebrafish were either exposed to vehicle (E3 medium), β-HB (1 mM), or NMN (50 µM)**.** At 48 hpf, all exposure conditions were washed out thrice and replaced by E3 medium. Zebrafish underwent behavioural assays at 2, 3 and 5 days-post fertilization (dpf). Briefly, zebrafish were placed in 48-well plates at a density of 1 fish/well. At 2 and 3 dpf, movement was analyzed in light and dark conditions via quantization assay within the ZebraBox® recording chamber (Viewpoint Life Sciences, Montreal, QC). At 5 dpf, locomotion was analyzed in light and dark via tracking assay using the ZebraBox®**.** After behavioural assays were completed, zebrafish were genotyped by PCR amplification of the *shank3b* gene with subsequent digestion with T7 endonuclease I (M0302; New England BioLabs). Genotypes were verified on a 2% agarose gel. Mismatched duplexes (seen as three bands on a gel) indicated a heterozygous genotype, whereas single banded samples required further DNA sequencing to indicate a wild type versus homozygous genotype.

Statistics: The statistical analysis of the data was performed using GraphPad Prism 9 (Version 9.4.1) software (La Jolla, CA, USA). All data are shown as mean ± SEM. Data were analyzed using t-test unless otherwise specified. The significant differences are presented as *** $p < 0.001$.

Figure Legends:

Figure 1: βHB and NMN promotes mitochondrial fusion and increases NAD^+ in Hela cell. (A) Representative confocal images of HeLa cells stained with antibodies against TOMM20 for mitochondrial network. HeLa cells were immuno-stained after 24h treatment with indicated concentrations of Veh or βHB or NMN or Eto+βHB. **(B)** Quantification of mean mitochondrial branch length were measured between Veh, βHB or NMN or Eto+βHB treated cells. This quantification was performed by Image-J, MiNA plugin from three independent replicates, using a standard region of interest (ROI) and measured randomly from each image. **(C)** Qualitative analysis of mitochondrial morphology was performed in Veh, βHB or NMN or Eto+βHB treated cells via an unbiased visual scoring method. Analysis was done using at least 150 cells per condition, and 3 independent replicates for each treatment condition. **(D)** NAD^+ level was measured 24h post treatment of Veh or βHB or NMN; and Veh or Eto+βHB in HeLa cells (n=3-6/group). Data are shown as mean ± SEM. Data were analyzed using t-test. The significant differences are presented as *** $p < 0.001$.

Figure 2: βHB and NMN acts on mitochondrial fusion machinery and peroxisome differently. (A) Representative blots are presented for the densitometry analysis for **(B)** OPA1 and **(C)** $pDRP^{s616}$ **(D)** total DRP(n=3/group). Separately conducted set of experiments are presented using a dotted line under the same graph. **(E)** Representative confocal images of HeLa cells stained with antibodies against PMP70 for peroxisomes. HeLa cells were immuno-stained after 24h treatment with indicated concentrations of Veh or βHB or Eto+βHB or NMN. **(F)** Quantification of mean number of peroxisomes per cell were measured between Veh, βHB or Eto+βHB or NMN treated

cells. This quantification was performed by Image-J, particle analysis feature, using a standard region of interest (ROI) and measured randomly from all images, with the particle analysis tool. **(G)** Quantitative analysis of sizes of peroxisomes for control and drug treatment(s) and concentration(s) mentioned. Analysis was done using at least 150 cells per condition, and 3 independent replicates for each treatment condition. Data are shown as mean ± SEM. Data were analyzed using t-test. The significant differences are presented as *** $p < 0.001$

Figure 3: βHB and NMN supplementation in HeLa cell reduces acetylation. (A) Representative blots are presented for the densitometry analysis for **(B)** global acetylation in Veh or βHB or NMN treated cells (n=3/group) along with Actin as the loading control; **(C)** acetylated-OPA1 and **(D)** acetylated-DRP1 normalised to input as control (n=3/group). Data are shown as mean ± SEM. Data were analyzed using t-test. The significant differences are presented as *** $p < 0.001$.

Figure 4: Inhibition of Sirtuin 1 and 2, blocks βHB and NMN aided mitochondrial fusion but not the peroxisome network (A) Representative confocal images of HeLa cells stained with antibodies against TOMM20 for mitochondrial network. HeLa cells were immuno-stained after 24h treatment with indicated concentrations of Veh (Vehicle) or Sirtinol or Sirtinol+βHB or Sirtinol+NMN. **(B)** Quantification of mean mitochondrial branch length and **(C)** Qualitative analysis of mitochondrial morphology were measured between Veh or Sirtinol, Sirtinol+βHB or Sirtinol+NMN treated cells. Analysis was done using at least 150 cells per condition, and 3 independent replicates for each treatment condition. **(D)** Representative confocal images of HeLa cells stained with antibodies against PMP70 for peroxisomes. HeLa cells were immuno-stained after

24h treatment with indicated concentrations of Veh (Vehicle) or Sirtinol or Sirtinol+βHB or Sirtinol+NMN. **(E)** Quantification of total number of peroxisomes per cell and **(F)** quantitative analysis of peroxisome size(s) were measured between Veh or Sirtinol, Sirtinol+βHB or Sirtinol+NMN treated cells. Analysis was done using at least 150 cells per condition, and 3 independent replicates for each treatment condition. Data are shown as mean ± SEM. Data were analyzed using t-test. The significant differences are presented as *** $p < 0.001$.

Figure 5: βHB promotes mitochondrial fusion via Sirt2 dependent manner. **(A)** Representative confocal images of HeLa cells stained with antibodies against TOMM20 for mitochondrial network. HeLa cells were immuno-stained 48h post transfection of siRNA targets. 24h post siRNA transfection, with indicated concentrations of βHB or NMN was added for 24h into each siRNA target group. Representative confocal images of HeLa cells stained with antibodies against TOMM20 for mitochondrial network in Sirt1 and Sirt2 KD cells with 24h post treatment of βHB or NMN. Quantification of mean mitochondrial branch length were measured between **(B)** Veh or βHB or NMN. This quantification was performed by Image-J, MiNA plugin from three independent replicates, using a standard region of interest (ROI) and measured randomly from each image. **(C)** Qualitative analysis of mitochondrial morphology was performed in Veh, βHB or NMN treated cells via an unbiased visual scoring method. Analysis was done using at least 80 cells per condition, and 2 technical replicates for each treatment condition. Data are shown as mean ± SEM. Data were analyzed using t-test. The significant differences are presented as *** $p < 0.001$.

Figure 6: NMN effects locomotion in zebrafish shank3b model A) Exposure and behavioural paradigm. **B)** Burst distance travelled (individually normalized to distance travelled under light) of 5 dpf *shank3b*$^{+/+}$ and *shank3b*$^{+/-}$ **(C)** Distance travelled (mm) of 5 dpf *shank3b*$^{+/+}$ and *shank3b*$^{+/-}$ zebrafish exposed to vehicle (Veh; E3), β-HB (1 mM), or NMN (50 µM) from 10-48 hpf under dark or **(D)** light conditions. Data are shown as mean ± SEM. n=14-71 fish. Data were analyzed using two-way ANOVA with post-hoc Tukey test. Relevant significant differences are presented on the figure.

Authors Contribution: GMU: designed the study, performed experiments, analysed data, coordinated experiments with other collaborators, generated figures, and wrote and edited the manuscript. RL: designed and performed fish behavioural assays (including breeding), analysed data, and contributed to writing and editing. MZ: performed the peroxisome assay and data analysis. IAK: provided technical support for microscopy and siRNA experiments. JMR: obtained funding, designed the study, and edited manuscript. DMK: designed the fish experiments and edited the manuscript. TES: obtained funding, designed and coordinated the study, and wrote and edited the manuscript as the corresponding author.

Acknowledgements: We thank Dr David A. Sinclair (Professor at the Department of Genetics and Co-Director of the Paul F. Glenn Center for Biology of Aging Research at Harvard Medical School) for kindly providing the NMN.

Ethics Approval: All fish protocols were approved by the University of Calgary Institutional Animal Care and Use Committee, which conform with the Guide for the Care and Use of Laboratory Animals published by the United States National Institutes of Health (eighth edition; revised 2011) and the guidelines of the Canadian Council on Animal Care.

Sources of Funding: This study was supported by funds from the Scottish Rites Charitable Foundation (TES, JMR), and the Alberta Children's Hospital Research Foundation Neurodevelopment Disorder Program (JMR, TES). MZ was supported by

Owerko Centre, University of Calgary. GMU was supported by an Alberta Children's Hospital Research Foundation - Cumming School of Medicine postdoctoral fellowship.

Conflict of interest: The authors have declared that no conflict of interest exists

Supplementary Materials:

Supplementary Figure 1: (A) Representative images for the visual scoring of mitochondrial morphology. **(B)** NAD^+ and **(C)** Total NAD^++NADH level was measured 24h post treatment of Veh or βHB or NMN n HeLa cells. **(D)** Representative blots are presented for the densitometry analysis for mitochondrial fusion and fission related protein expression of **(E)** MFN1, **(F)** MFN2, **(G)** MFF in Veh, and βHB or NMN treated cells (n=3/group). Data are shown as mean ± SEM. Data were analyzed using t-test. The significant differences are presented as *** $p < 0.001$.

Supplementary Figure 2: (A) Representative confocal images of HeLa cells stained with antibodies against TOMM20 for mitochondrial network. HeLa cells were immuno-stained after 24h treatment with indicated concentrations of Veh or βHB or Eto or Eto+βHB. **(B)** Quantification of mitochondrial average branch length were measured between Veh or βHB or Eto or Eto+βHB treated cells. This quantification was performed by Image-J, MiNA plugin from three independent replicates, using a standard region of interest (ROI) and measured randomly from each image. **(C)** Qualitative analysis of mitochondrial morphology was performed in Veh or βHB or Eto or Eto+βHB treated cells via an unbiased visual scoring method. Analysis was done using at least 150 cells per condition, and 3 independent replicates for each treatment condition. **(D, E)** NAD^+ and total

NAD^++NADH level was measured 24h post treatment of Veh, βHB, Eto or Eto+βHB. **(F, G)** Representative blots of global acetylation in Veh, or sirtinol treated cells for 24h (n=3/group) along with Actin as the loading control and their densitometric analysis. **(H, I**) NAD^+ and total NAD^++NADH level was measured 24h post treatment of Veh, Sirtinol, Sirtinol+βHB or Sirtinol+NMN in HeLa cells respectively. Data are shown as mean ± SEM. Data were analyzed using t-test. The significant differences are presented as *** $p < 0.001$.

Supplementary Figure 3: (A) Representative confocal images of HeLa cells stained with antibodies against TOMM20 for mitochondrial network. **(A)** The HeLa cells were immuno-stained 48h post transfection of siSirt1 (target1, target 2 and target 3). 24h post siRNA transfection, with indicated concentrations of βHB or NMN was added for 24h into each siRNA target group. **(B)** Quantification of mitochondrial average branch length were measured between the indicated groups in each siRNA targets. This quantification was performed by Image-J, MiNA plugin from three independent replicates, using a standard region of interest (ROI) and measured randomly from each image. **(C)** Qualitative quantification of mitochondrial morphology was performed between the indicated groups in each siRNA targets via an unbiased visual scoring method. Analysis was done using at least 80 cells per condition, and 2 technical replicates for each treatment condition. Data are shown as mean ± SEM. Data were analyzed using t-test. The significant differences are presented as *** $p < 0.001$.

Supplementary Figure 4: (A) Representative confocal images of HeLa cells stained with antibodies against TOMM20 for mitochondrial network. **(A)** The HeLa cells were immuno-stained 48h post transfection of siSirt2 (target1, target 2 and target 3). 24h post siRNA

transfection, with indicated concentrations of βHB or NMN was added for 24h into each siRNA target group. **(B)** Quantification of mitochondrial average branch length were measured between the indicated groups in each siRNA targets. This quantification was performed by Image-J, MiNA plugin from three independent replicates, using a standard region of interest (ROI) and measured randomly from each image. **(C)** Qualitative quantification of mitochondrial morphology was performed between the indicated groups in each siRNA targets via an unbiased visual scoring method. Analysis was done using at least 80 cells per condition, and 2 technical replicates for each treatment condition. Data are shown as mean ± SEM. Data were analyzed using t-test. The significant differences are presented as *** $p < 0.001$.

Supplementary Figure 5: (A) Representative confocal images of HeLa cells stained with antibodies against TOMM20 for mitochondrial network. **(A)** The HeLa cells were immuno-stained 48h post transfection of siSirt3 (target1, target 2 and target 3). 24h post siRNA transfection, with indicated concentrations of βHB or NMN was added for 24h into each siRNA target group. **(B)** Quantification of mitochondrial average branch length were measured between the indicated groups in each siRNA targets. This quantification was performed by Image-J, MiNA plugin from three independent replicates, using a standard region of interest (ROI) and measured randomly from each image. **(C)** Qualitative quantification of mitochondrial morphology was performed between the indicated groups in each siRNA targets via an unbiased visual scoring method. Analysis was done using at least 80 cells per condition, and 2 technical replicates for each treatment condition. Data are shown as mean ± SEM. Data were analyzed using t-test. The significant differences are presented as *** $p < 0.001$.

Supplementary Figure 6: (A-F) Original blots presented that was used to present the representative bands in analysis and figures.

References

Ahn, Sabouny, R., Villa, B. R., Yee, N. C., Mychasiuk, R., Uddin, G. M., . . . Shutt, T. E. (2020). Aberrant Mitochondrial Morphology and Function in the BTBR Mouse Model of Autism Is Improved by Two Weeks of Ketogenic Diet. *Int J Mol Sci, 21*(9). doi:10.3390/ijms21093266

Ahn, Y., Narous, M., Tobias, R., Rho, J. M., & Mychasiuk, R. (2014). The ketogenic diet modifies social and metabolic alterations identified in the prenatal valproic acid model of autism spectrum disorder. *Dev Neurosci, 36*(5), 371-380. doi:10.1159/000362645

Ahn, Y., Sabouny, R., Villa, B. R., Yee, N. C., Mychasiuk, R., Uddin, G. M., . . . Shutt, T. E. (2020). Aberrant mitochondrial morphology and function in the BTBR mouse model of autism is improved by two weeks of ketogenic diet. *International journal of molecular sciences, 21*(9), 3266.

Baker, N., Patel, J., & Khacho, M. (2019). Linking mitochondrial dynamics, cristae remodeling and supercomplex formation: how mitochondrial structure can regulate bioenergetics. *Mitochondrion, 49*, 259-268.

Barone, R., Bastin, J., Djouadi, F., Singh, I., Karim, M. A., Ammanamanchi, A., . . . Frye, R. E. (2021). Mitochondrial Fatty Acid beta-Oxidation and Resveratrol Effect in Fibroblasts from Patients with Autism Spectrum Disorder. *J Pers Med, 11*(6). doi:10.3390/jpm11060510

Biel, T. G., Lee, S., Flores-Toro, J. A., Dean, J. W., Go, K. L., Lee, M. H., . . . Kim, J. S. (2016). Sirtuin 1 suppresses mitochondrial dysfunction of ischemic mouse livers in a mitofusin 2-dependent manner. *Cell Death Differ, 23*(2), 279-290. doi:10.1038/cdd.2015.96

Bonkowski, M. S., & Sinclair, D. A. (2016). Slowing ageing by design: the rise of NAD(+) and sirtuin-activating compounds. *Nat Rev Mol Cell Biol, 17*(11), 679-690. doi:10.1038/nrm.2016.93

Chan, D. C. (2020). Mitochondrial dynamics and its involvement in disease. *Annual review of pathology: mechanisms of disease, 15*, 235-259.

Citrigno, L., Muglia, M., Qualtieri, A., Spadafora, P., Cavalcanti, F., Pioggia, G., & Cerasa, A. (2020). The Mitochondrial Dysfunction Hypothesis in Autism Spectrum Disorders: Current Status and Future Perspectives. *Int J Mol Sci, 21*(16). doi:10.3390/ijms21165785

Covarrubias, A. J., Perrone, R., Grozio, A., & Verdin, E. (2021). NAD(+) metabolism and its roles in cellular processes during ageing. *Nat Rev Mol Cell Biol, 22*(2), 119-141. doi:10.1038/s41580-020-00313-x

Dreyer, C., Keller, H., Mahfoudi, A., Laudet, V., Krey, G., & Wahli, W. (1993). Positive regulation of the peroxisomal beta-oxidation pathway by fatty acids through activation of peroxisome proliferator-activated receptors (PPAR). *Biol Cell, 77*(1), 67-76. doi:10.1016/s0248-4900(05)80176-5

Durand, C. M., Betancur, C., Boeckers, T. M., Bockmann, J., Chaste, P., Fauchereau, F., . . . Bourgeron, T. (2007). Mutations in the gene encoding the synaptic scaffolding protein SHANK3 are associated with autism spectrum disorders. *Nat Genet, 39*(1), 25-27. doi:10.1038/ng1933

El-Rashidy, O., El-Baz, F., El-Gendy, Y., Khalaf, R., Reda, D., & Saad, K. (2017). Ketogenic diet versus gluten free casein free diet in autistic children: a case-control study. *Metab Brain Dis, 32*(6), 1935-1941. doi:10.1007/s11011-017-0088-z

716 Elamin, M., Ruskin, D. N., Masino, S. A., & Sacchetti, P. (2017). Ketone-Based Metabolic Therapy: Is
717 Increased NAD(+) a Primary Mechanism? *Front Mol Neurosci, 10*, 377.
718 doi:10.3389/fnmol.2017.00377
719 Evangeliou, A., Vlachonikolis, I., Mihailidou, H., Spilioti, M., Skarpalezou, A., Makaronas, N., . . . Smeitink,
720 J. (2003). Application of a ketogenic diet in children with autistic behavior: pilot study. *J Child*
721 *Neurol, 18*(2), 113-118. doi:10.1177/08830738030180020501
722 Frye, R. E., Lionnard, L., Singh, I., Karim, M. A., Chajra, H., Frechet, M., . . . Aouacheria, A. (2021).
723 Mitochondrial morphology is associated with respiratory chain uncoupling in autism spectrum
724 disorder. *Transl Psychiatry, 11*(1), 527. doi:10.1038/s41398-021-01647-6
725 Galmozzi, A., Mitro, N., Ferrari, A., Gers, E., Gilardi, F., Godio, C., . . . Crestani, M. (2013). Inhibition of
726 class I histone deacetylases unveils a mitochondrial signature and enhances oxidative
727 metabolism in skeletal muscle and adipose tissue. *Diabetes, 62*(3), 732-742. doi:10.2337/db12-
728 0548
729 Gevezova, M., Minchev, D., Pacheva, I., Sbirkov, Y., Yordanova, R., Timova, E., . . . Sarafian, V. (2021).
730 Cellular Bioenergetic and Metabolic Changes in Patients with Autism Spectrum Disorder. *Curr*
731 *Top Med Chem, 21*(11), 985-994. doi:10.2174/1568026621666210521142131
732 Gilmour, B. C., Gudmundsrud, R., Frank, J., Hov, A., Lautrup, S., Aman, Y., . . . Fang, E. F. (2020). Targeting
733 NAD(+) in translational research to relieve diseases and conditions of metabolic stress and
734 ageing. *Mech Ageing Dev, 186*, 111208. doi:10.1016/j.mad.2020.111208
735 Glancy, B., Kim, Y., Katti, P., & Willingham, T. B. (2020). The functional impact of mitochondrial structure
736 across subcellular scales. *Frontiers in physiology, 11*.
737 Gogou, M., & Kolios, G. (2018). Are therapeutic diets an emerging additional choice in autism spectrum
738 disorder management? *World J Pediatr, 14*(3), 215-223. doi:10.1007/s12519-018-0164-4
739 Hess, R., Staubli, W., & Riess, W. (1965). Nature of the hepatomegalic effect produced by ethyl-
740 chlorophenoxy-isobutyrate in the rat. *Nature, 208*(5013), 856-858. doi:10.1038/208856a0
741 Hu, Q., Zhang, H., Gutierrez Cortes, N., Wu, D., Wang, P., Zhang, J., . . . Wang, W. (2020). Increased Drp1
742 Acetylation by Lipid Overload Induces Cardiomyocyte Death and Heart Dysfunction. *Circ Res,*
743 *126*(4), 456-470. doi:10.1161/CIRCRESAHA.119.315252
744 Ilieva, M., Aldana, B. I., Vinten, K. T., Hohmann, S., Woofenden, T. W., Lukjanska, R., . . . Michel, T. M.
745 (2022). Proteomic phenotype of cerebral organoids derived from autism spectrum disorder
746 patients reveal disrupted energy metabolism, cellular components, and biological processes.
747 *Mol Psychiatry*. doi:10.1038/s41380-022-01627-2
748 Kalueff, A. V., Stewart, A. M., & Gerlai, R. (2014). Zebrafish as an emerging model for studying complex
749 brain disorders. *Trends Pharmacol Sci, 35*(2), 63-75. doi:10.1016/j.tips.2013.12.002
750 Kang, H. C., Chung, D. E., Kim, D. W., & Kim, H. D. (2004). Early- and late-onset complications of the
751 ketogenic diet for intractable epilepsy. *Epilepsia, 45*(9), 1116-1123. doi:10.1111/j.0013-
752 9580.2004.10004.x
753 Kartawy, M., Khaliulin, I., & Amal, H. (2021). Systems Biology Reveals S-Nitrosylation-Dependent
754 Regulation of Mitochondrial Functions in Mice with Shank3 Mutation Associated with Autism
755 Spectrum Disorder. *Brain Sci, 11*(6). doi:10.3390/brainsci11060677
756 Kashiwaya, Y., Takeshima, T., Mori, N., Nakashima, K., Clarke, K., & Veech, R. L. (2000). D-beta-
757 hydroxybutyrate protects neurons in models of Alzheimer's and Parkinson's disease. *Proc Natl*
758 *Acad Sci U S A, 97*(10), 5440-5444. doi:10.1073/pnas.97.10.5440
759 Klimova, N., Long, A., & Kristian, T. (2019). Nicotinamide mononucleotide alters mitochondrial dynamics
760 by SIRT3-dependent mechanism in male mice. *J Neurosci Res, 97*(8), 975-990.
761 doi:10.1002/jnr.24397

762 Lee, Kapur, M., Li, M., Choi, M. C., Choi, S., Kim, H. J., . . . Yao, T. P. (2014). MFN1 deacetylation activates
763 adaptive mitochondrial fusion and protects metabolically challenged mitochondria. *J Cell Sci,*
764 *127*(Pt 22), 4954-4963. doi:10.1242/jcs.157321
765 Lee, R. W. Y., Corley, M. J., Pang, A., Arakaki, G., Abbott, L., Nishimoto, M., . . . Wong, M. (2018). A
766 modified ketogenic gluten-free diet with MCT improves behavior in children with autism
767 spectrum disorder. *Physiol Behav, 188*, 205-211. doi:10.1016/j.physbeh.2018.02.006
768 Lee, S., Chun, H. S., Lee, J., Park, H. J., Kim, K. T., Kim, C. H., . . . Kim, W. K. (2018). Plausibility of the
769 zebrafish embryos/larvae as an alternative animal model for autism: A comparison study of
770 transcriptome changes. *PLoS One, 13*(9), e0203543. doi:10.1371/journal.pone.0203543
771 Lee, Y., Ryu, J. R., Kang, H., Kim, Y., Kim, S., Zhang, Y., . . . Han, K. (2017). Characterization of the zinc-
772 induced Shank3 interactome of mouse synaptosome. *Biochem Biophys Res Commun, 494*(3-4),
773 581-586. doi:10.1016/j.bbrc.2017.10.143
774 Lin, A., Turner, Z., Doerrer, S. C., Stanfield, A., & Kossoff, E. H. (2017). Complications During Ketogenic
775 Diet Initiation: Prevalence, Treatment, and Influence on Seizure Outcomes. *Pediatr Neurol, 68*,
776 35-39. doi:10.1016/j.pediatrneurol.2017.01.007
777 Liu, C. X., Li, C. Y., Hu, C. C., Wang, Y., Lin, J., Jiang, Y. H., . . . Xu, X. (2018). CRISPR/Cas9-induced shank3b
778 mutant zebrafish display autism-like behaviors. *Mol Autism, 9*, 23. doi:10.1186/s13229-018-
779 0204-x
780 Lopaschuk, G. D., Karwi, Q. G., Ho, K. L., Pherwani, S., & Ketema, E. B. (2020). Ketone metabolism in the
781 failing heart. *Biochim Biophys Acta Mol Cell Biol Lipids, 1865*(12), 158813.
782 doi:10.1016/j.bbalip.2020.158813
783 Mai, A., Massa, S., Lavu, S., Pezzi, R., Simeoni, S., Ragno, R., . . . Sinclair, D. A. (2005). Design, synthesis,
784 and biological evaluation of sirtinol analogues as class III histone/protein deacetylase (Sirtuin)
785 inhibitors. *J Med Chem, 48*(24), 7789-7795. doi:10.1021/jm050100l
786 Miyamoto, J., Ohue-Kitano, R., Mukouyama, H., Nishida, A., Watanabe, K., Igarashi, M., . . . Kimura, I.
787 (2019). Ketone body receptor GPR43 regulates lipid metabolism under ketogenic conditions.
788 *Proc Natl Acad Sci U S A, 116*(47), 23813-23821. doi:10.1073/pnas.1912573116
789 Monteiro, P., & Feng, G. (2017). SHANK proteins: roles at the synapse and in autism spectrum disorder.
790 *Nat Rev Neurosci, 18*(3), 147-157. doi:10.1038/nrn.2016.183
791 Napoli, E., Duenas, N., & Giulivi, C. (2014). Potential therapeutic use of the ketogenic diet in autism
792 spectrum disorders. *Front Pediatr, 2*, 69. doi:10.3389/fped.2014.00069
793 Neal, E. G., Chaffe, H., Schwartz, R. H., Lawson, M. S., Edwards, N., Fitzsimmons, G., . . . Cross, J. H.
794 (2008). The ketogenic diet for the treatment of childhood epilepsy: a randomised controlled
795 trial. *Lancet Neurol, 7*(6), 500-506. doi:10.1016/S1474-4422(08)70092-9
796 Newman, J. C., & Verdin, E. (2014). beta-hydroxybutyrate: much more than a metabolite. *Diabetes Res*
797 *Clin Pract, 106*(2), 173-181. doi:10.1016/j.diabres.2014.08.009
798 Newman, J. C., & Verdin, E. (2017). beta-Hydroxybutyrate: A Signaling Metabolite. *Annu Rev Nutr, 37*,
799 51-76. doi:10.1146/annurev-nutr-071816-064916
800 Oanh, N. T. K., Park, Y. Y., & Cho, H. (2017). Mitochondria elongation is mediated through SIRT1-
801 mediated MFN1 stabilization. *Cell Signal, 38*, 67-75. doi:10.1016/j.cellsig.2017.06.019
802 Pecorelli, A., Ferrara, F., Messano, N., Cordone, V., Schiavone, M. L., Cervellati, F., . . . Valacchi, G. (2020).
803 Alterations of mitochondrial bioenergetics, dynamics, and morphology support the theory of
804 oxidative damage involvement in autism spectrum disorder. *FASEB J, 34*(5), 6521-6538.
805 doi:10.1096/fj.201902677R
806 Rossignol, D. A., & Frye, R. E. (2012). Mitochondrial dysfunction in autism spectrum disorders: a
807 systematic review and meta-analysis. *Mol Psychiatry, 17*(3), 290-314. doi:10.1038/mp.2010.136

808 Ruskin, D. N., Murphy, M. I., Slade, S. L., & Masino, S. A. (2017). Ketogenic diet improves behaviors in a
809 maternal immune activation model of autism spectrum disorder. *PLoS One, 12*(2), e0171643.
810 doi:10.1371/journal.pone.0171643
811 Ruskin, D. N., Svedova, J., Cote, J. L., Sandau, U., Rho, J. M., Kawamura, M., Jr., . . . Masino, S. A. (2013).
812 Ketogenic diet improves core symptoms of autism in BTBR mice. *PLoS One, 8*(6), e65021.
813 doi:10.1371/journal.pone.0065021
814 Sabouny, R., & Shutt, T. E. (2020). Reciprocal Regulation of Mitochondrial Fission and Fusion. *Trends*
815 *Biochem Sci, 45*(7), 564-577. doi:10.1016/j.tibs.2020.03.009
816 Samant, S. A., Zhang, H. J., Hong, Z., Pillai, V. B., Sundaresan, N. R., Wolfgeher, D., . . . Gupta, M. P.
817 (2014). SIRT3 deacetylates and activates OPA1 to regulate mitochondrial dynamics during stress.
818 *Mol Cell Biol, 34*(5), 807-819. doi:10.1128/MCB.01483-13
819 Santra, S., Gilkerson, R. W., Davidson, M., & Schon, E. A. (2004). Ketogenic treatment reduces deleted
820 mitochondrial DNAs in cultured human cells. *Ann Neurol, 56*(5), 662-669.
821 doi:10.1002/ana.20240
822 Sheng, X., & Cristea, I. M. (2021). The antiviral sirtuin 3 bridges protein acetylation to mitochondrial
823 integrity and metabolism during human cytomegalovirus infection. *PLoS Pathog, 17*(4),
824 e1009506. doi:10.1371/journal.ppat.1009506
825 Shimazu, T., Hirschey, M. D., Newman, J., He, W., Shirakawa, K., Le Moan, N., . . . Verdin, E. (2013).
826 Suppression of oxidative stress by beta-hydroxybutyrate, an endogenous histone deacetylase
827 inhibitor. *Science, 339*(6116), 211-214. doi:10.1126/science.1227166
828 Shutt, T. E., & McBride, H. M. (2013). Staying cool in difficult times: mitochondrial dynamics, quality
829 control and the stress response. *Biochim Biophys Acta, 1833*(2), 417-424.
830 doi:10.1016/j.bbamcr.2012.05.024
831 Singh, K., Singh, I. N., Diggins, E., Connors, S. L., Karim, M. A., Lee, D., . . . Frye, R. E. (2020).
832 Developmental regression and mitochondrial function in children with autism. *Ann Clin Transl*
833 *Neurol, 7*(5), 683-694. doi:10.1002/acn3.51034
834 Spilioti, M., Evangeliou, A. E., Tramma, D., Theodoridou, Z., Metaxas, S., Michailidi, E., . . . Gibson, K. M.
835 (2013). Evidence for treatable inborn errors of metabolism in a cohort of 187 Greek patients
836 with autism spectrum disorder (ASD). *Front Hum Neurosci, 7*, 858.
837 doi:10.3389/fnhum.2013.00858
838 Tang, G., Gutierrez Rios, P., Kuo, S. H., Akman, H. O., Rosoklija, G., Tanji, K., . . . Sulzer, D. (2013).
839 Mitochondrial abnormalities in temporal lobe of autistic brain. *Neurobiol Dis, 54*, 349-361.
840 doi:10.1016/j.nbd.2013.01.006
841 Thorsen, M. (2020). Oxidative stress, metabolic and mitochondrial abnormalities associated with autism
842 spectrum disorder. *Prog Mol Biol Transl Sci, 173*, 331-354. doi:10.1016/bs.pmbts.2020.04.018
843 Uddin, G. M., Abbas, R., & Shutt, T. E. (2021). The role of protein acetylation in regulating mitochondrial
844 fusion and fission. *Biochem Soc Trans, 49*(6), 2807-2819. doi:10.1042/BST20210798
845 Valente, A. J., Maddalena, L. A., Robb, E. L., Moradi, F., & Stuart, J. A. (2017). A simple ImageJ macro tool
846 for analyzing mitochondrial network morphology in mammalian cell culture. *Acta Histochem,*
847 *119*(3), 315-326. doi:10.1016/j.acthis.2017.03.001
848 Wai, T., & Langer, T. (2016). Mitochondrial Dynamics and Metabolic Regulation. *Trends Endocrinol*
849 *Metab, 27*(2), 105-117. doi:10.1016/j.tem.2015.12.001
850 Weber, D. D., Aminzadeh-Gohari, S., Tulipan, J., Catalano, L., Feichtinger, R. G., & Kofler, B. (2020).
851 Ketogenic diet in the treatment of cancer - Where do we stand? *Mol Metab, 33*, 102-121.
852 doi:10.1016/j.molmet.2019.06.026
853 Weissman, J. R., Kelley, R. I., Bauman, M. L., Cohen, B. H., Murray, K. F., Mitchell, R. L., . . . Natowicz, M.
854 R. (2008). Mitochondrial disease in autism spectrum disorder patients: a cohort analysis. *PLoS*
855 *One, 3*(11), e3815. doi:10.1371/journal.pone.0003815

856 Whitley, B. N., Engelhart, E. A., & Hoppins, S. (2019). Mitochondrial dynamics and their potential as a
857 therapeutic target. *Mitochondrion, 49*, 269-283. doi:10.1016/j.mito.2019.06.002
858 Xu, F. Y., Taylor, W. A., Hurd, J. A., & Hatch, G. M. (2003). Etomoxir mediates differential metabolic
859 channeling of fatty acid and glycerol precursors into cardiolipin in H9c2 cells. *J Lipid Res, 44*(2),
860 415-423. doi:10.1194/jlr.M200335-JLR200
861 Yang, H., Sibilla, C., Liu, R., Yun, J., Hay, B. A., Blackstone, C., . . . Guo, M. (2022). Clueless/CLUH regulates
862 mitochondrial fission by promoting recruitment of Drp1 to mitochondria. *Nat Commun, 13*(1),
863 1582. doi:10.1038/s41467-022-29071-4
864 Zhao, Z., Lange, D. J., Voustianiouk, A., MacGrogan, D., Ho, L., Suh, J., . . . Pasinetti, G. M. (2006). A
865 ketogenic diet as a potential novel therapeutic intervention in amyotrophic lateral sclerosis.
866 *BMC Neurosci, 7*, 29. doi:10.1186/1471-2202-7-29
867 Zhu, C. T., & Rand, D. M. (2012). A hydrazine coupled cycling assay validates the decrease in redox ratio
868 under starvation in Drosophila. *PLoS One, 7*(10), e47584. doi:10.1371/journal.pone.0047584

869

Figure 1

A

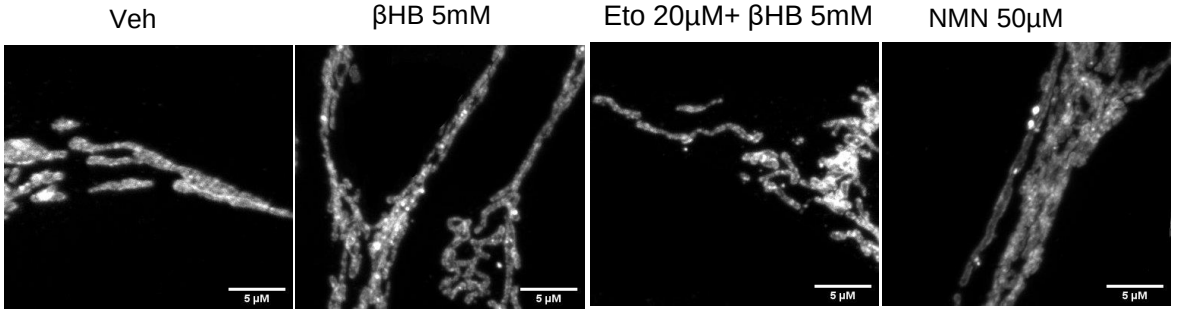

B

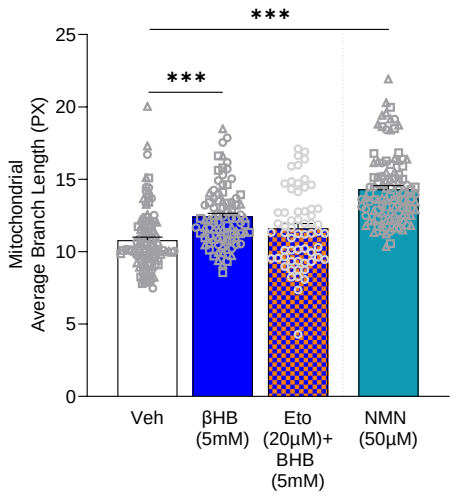

C

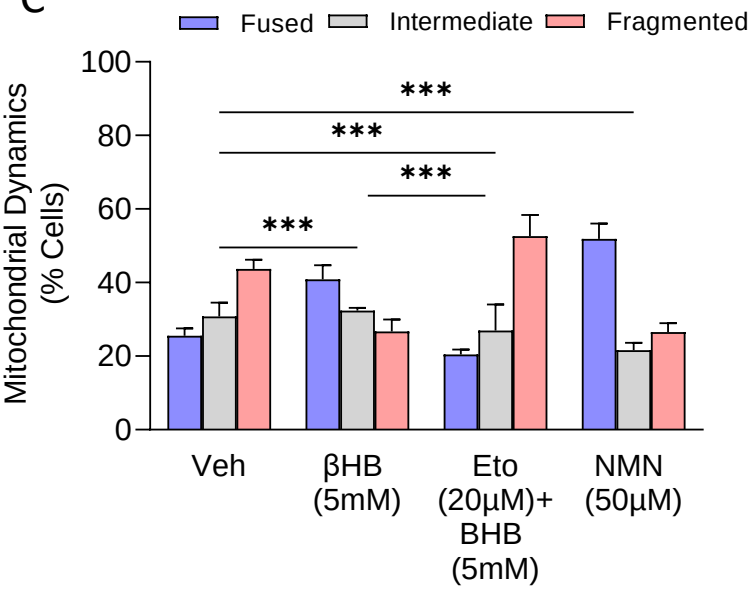

D

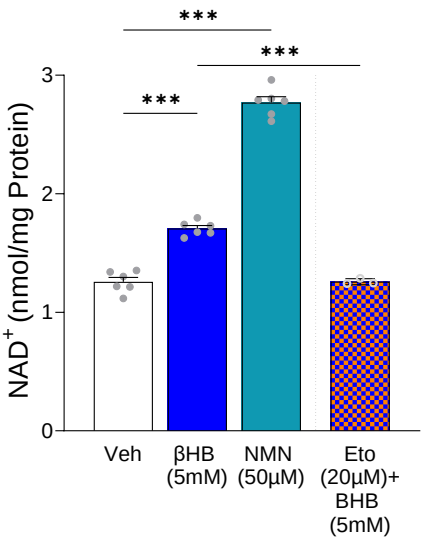

Figure 2

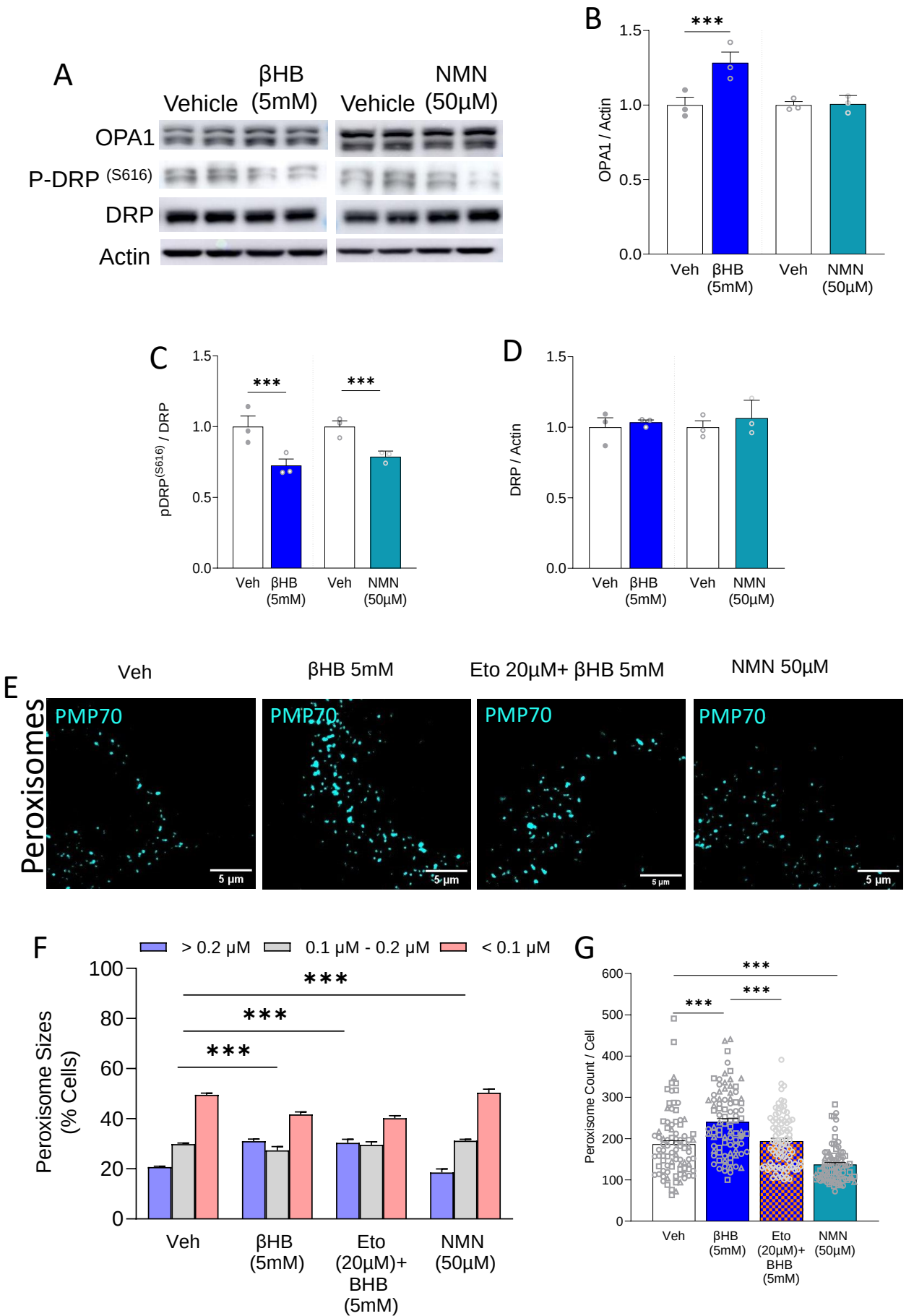
A
Vehicle
βHB (5mM)
Vehicle
NMN (50μM)
OPA1
P-DRP (S616)
DRP
Actin
B
OPA1 / Actin
***
Veh
βHB (5mM)
Veh
NMN (50μM)
C
pDRP(S616) / DRP
***
***
D
DRP / Actin
E
Veh
βHB 5mM
Eto 20μM+ βHB 5mM
NMN 50μM
Peroxisomes
PMP70
5 μm
F
> 0.2 μM
0.1 μM - 0.2 μM
< 0.1 μM
Peroxisome Sizes (% Cells)
***
Veh
βHB (5mM)
Eto (20μM)+ BHB (5mM)
NMN (50μM)
G
Peroxisome Count / Cell

Figure 3

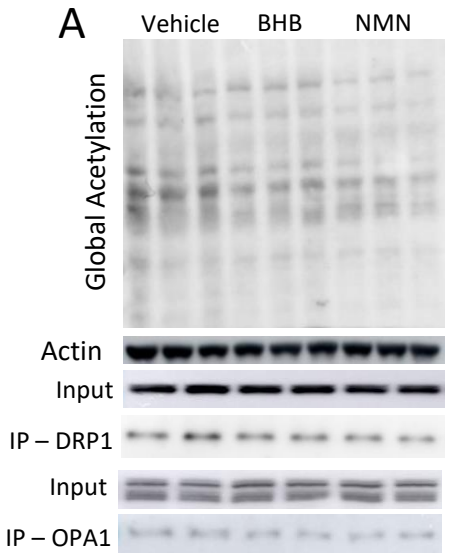
A
Vehicle
BHB
NMN
Global Acetylation
Actin
Input
IP – DRP1
Input
IP – OPA1

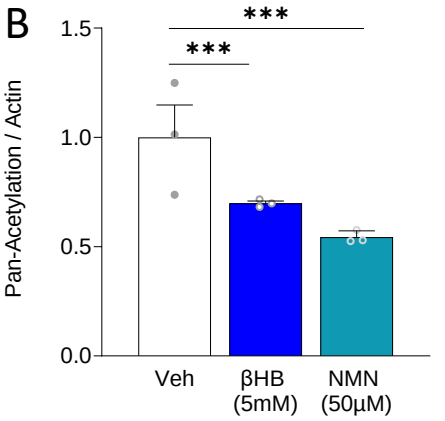
B
Pan-Acetylation / Actin
1.5
1.0
0.5
0.0
***
***
Veh
βHB (5mM)
NMN (50μM)

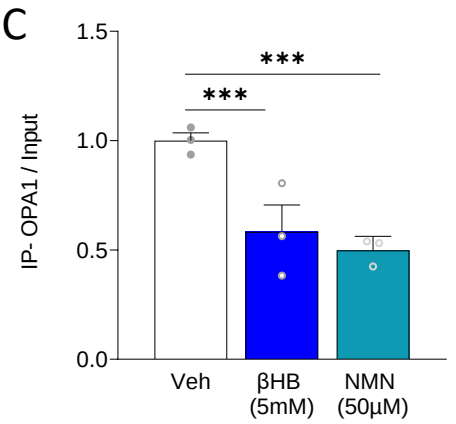
C
IP- OPA1 / Input
1.5
1.0
0.5
0.0
***
***
Veh
βHB (5mM)
NMN (50μM)

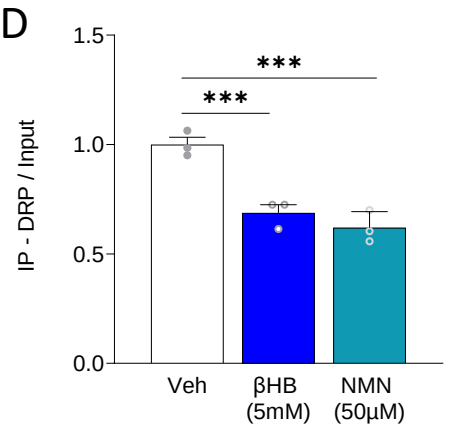
D
IP - DRP / Input
1.5
1.0
0.5
0.0
***
***
Veh
βHB (5mM)
NMN (50μM)

Figure 4

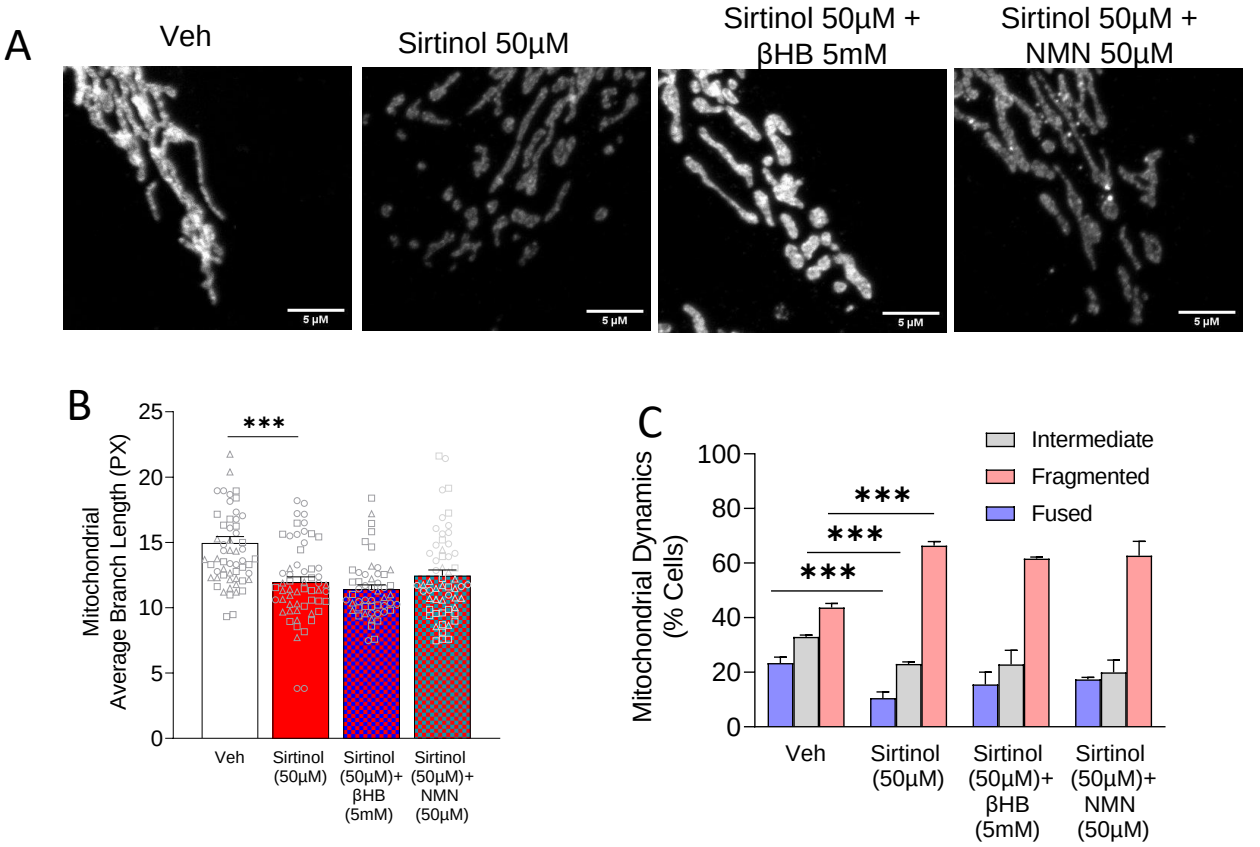
A
Veh
Sirtinol 50µM
Sirtinol 50µM + βHB 5mM
Sirtinol 50µM + NMN 50µM
5 µM
B
Mitochondrial Average Branch Length (PX)
25
20
15
10
5
0
***
Veh
Sirtinol (50µM)
Sirtinol (50µM)+ βHB (5mM)
Sirtinol (50µM)+ NMN (50µM)
C
Mitochondrial Dynamics (% Cells)
100
80
60
40
20
0
Intermediate
Fragmented
Fused
***
***
***
Veh
Sirtinol (50µM)
Sirtinol (50µM)+ βHB (5mM)
Sirtinol (50µM)+ NMN (50µM)

Figure 5

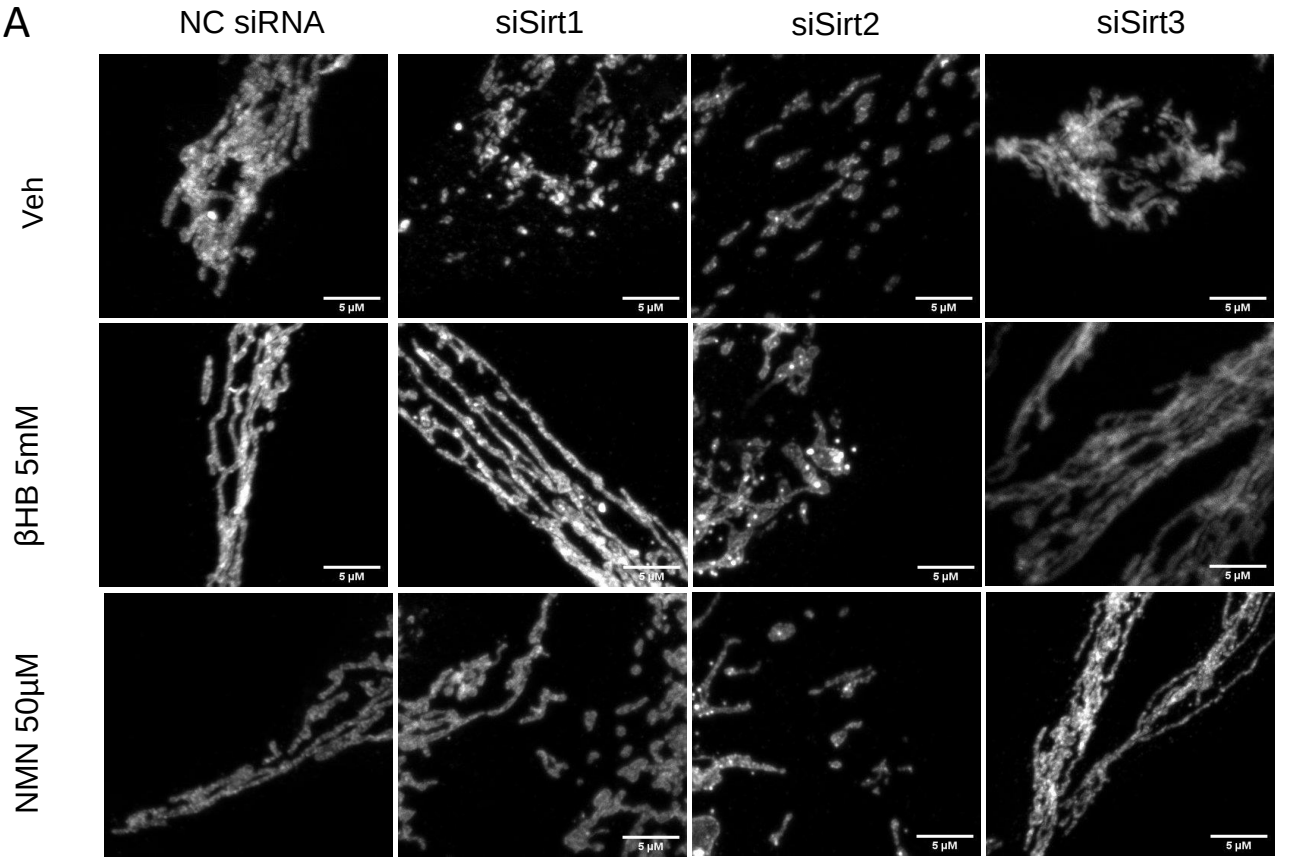
A
NC siRNA
siSirt1
siSirt2
siSirt3
Veh
βHB 5mM
NMN 50μM
5 μM

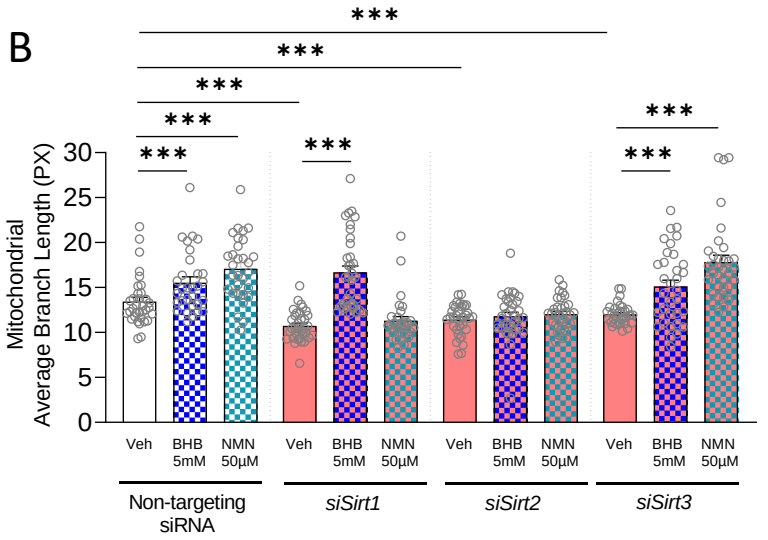
B
Mitochondrial Average Branch Length (PX)
30
25
20
15
10
5
0
***
Veh
BHB 5mM
NMN 50μM
Non-targeting siRNA
siSirt1
siSirt2
siSirt3

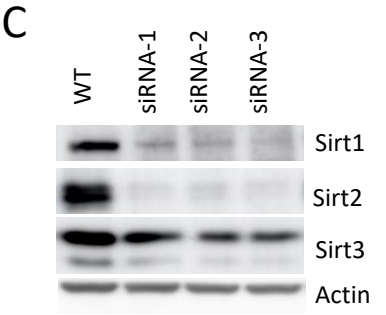
C
WT
siRNA-1
siRNA-2
siRNA-3
Sirt1
Sirt2
Sirt3
Actin

Figure 6

A

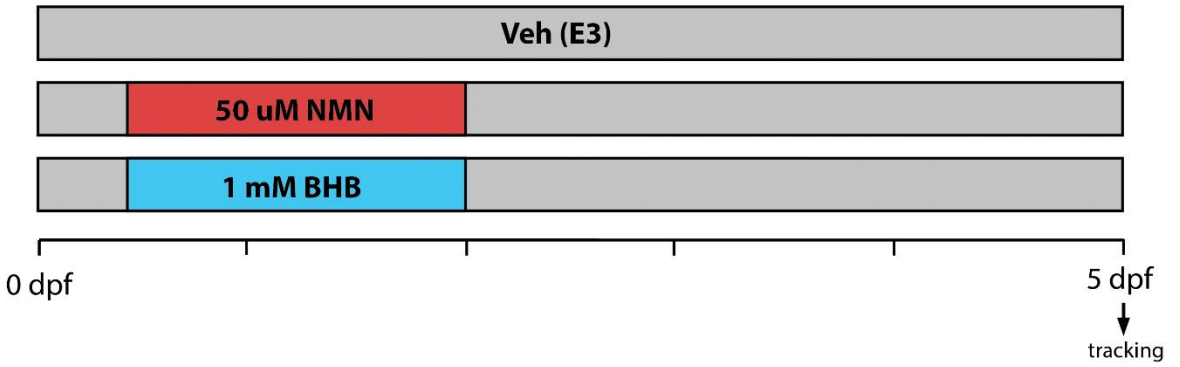

B

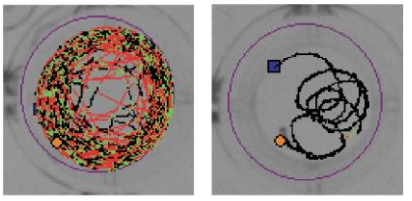

shank3b$^{+/+}$ *shank3b*$^{+/-}$

C

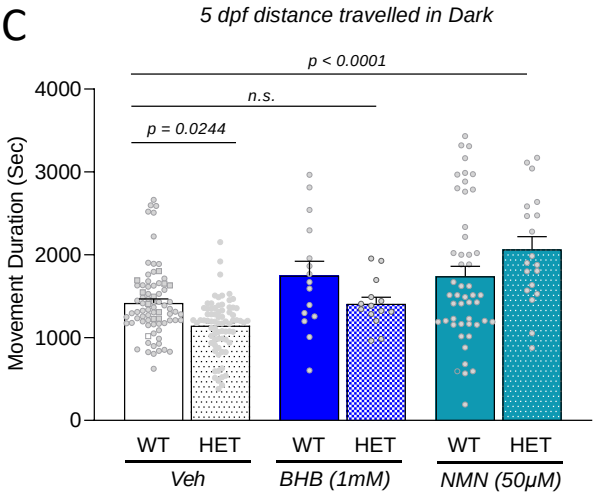
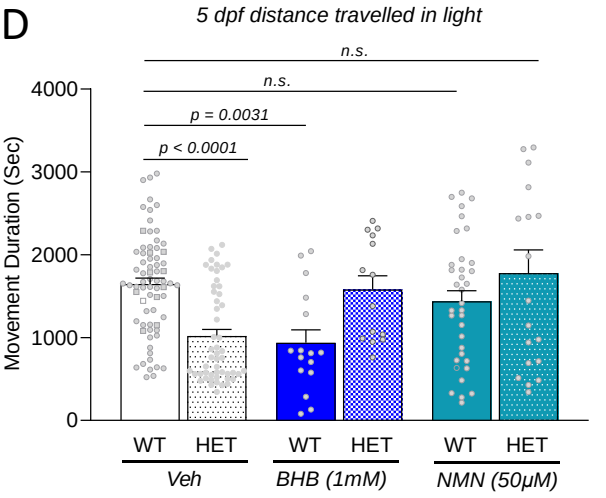
D